IOPscience iopscience.iop.org

Home Search Collections Journals About Contact us My IOPscience

Three types of site of Mn^{2+} in ZnS:Mn^{2+} nanocrystal/Pyrex glass composites

This article has been downloaded from IOPscience. Please scroll down to see the full text article.

1999 J. Phys.: Condens. Matter 11 5377

(http://iopscience.iop.org/0953-8984/11/27/313)

View the table of contents for this issue, or go to the journal homepage for more

Download details:
IP Address: 171.66.16.214
The article was downloaded on 15/05/2010 at 12:06

Please note that terms and conditions apply.

J. Phys.: Condens. Matter **11** (1999) 5377–5384. Printed in the UK PII: S0953-8984(99)00912-1

Three types of site of Mn^{2+} in ZnS:Mn^{2+} nanocrystal/Pyrex glass composites

Junye Liu†§, Chunxu Liu†, Yingguang Zheng‡, Dan Li†, Wu Xu† and Jiaqi Yu†

† Changchun Institute of Physics, Laboratory of Excited State Processes, Chinese Academy of Sciences, Changchun 130021, People's Republic of China
‡ Analysis Test and Experiment Center, Jilin University, Changchun 130023, People's Republic of China

E-mail: jyliu@public.cc.jl.cn

Received 13 January 1999, in final form 12 April 1999

Abstract. ZnS:Mn^{2+} nanocrystals embedded in Pyrex glass matrices have been studied systematically. It has been found by photoluminescence (PL) and excitation (PLE) spectra that doped Mn impurities can be classified as two types, occupying substitutional sites $(Mn^{2+})_{sub}$ and interstitial sites $(Mn^{2+})_{int}$. EPR experiments support this conclusion. In addition, Mn clusters were also identified from the EPR spectra. We observed the increases in the g_1 factors and hyperfine structure (HFS) constants with decreasing diameters of the nanocrystals. These increases are due to the hybridization between s–p states of ZnS and d states of the Mn ions by quantum confinement effects and the surface states.

1. Introduction

ZnS:Mn^{2+} bulk powder has been used as one of traditional electroluminescence phosphors for a long time. Ever since ZnS:Mn^{2+} nanocrystallites with high quantum efficiency (up to 18%) and a luminescence lifetime five orders of magnitude faster than in bulk ZnS were reported in 1994 [1], many investigations [2–4] have been directed at the understanding of the underlying physics of this high efficiency and fast radiation. The preparation and optical properties of the glasses doped with intrinsic semiconductors were extensively studied. But the reports on the glasses with dispersed doped semiconductor are very few. The glasses with dispersed nanoparticles have interesting properties which make them potential candidates for many technological applications, such as optical switches, bistability and waveguides. In this paper, we report in detail the optical and EPR spectra of ZnS:Mn^{2+} nanoparticle-doped glasses, and focus on the differences between ZnS:Mn^{2+}nanocrystallites and bulk powder in spectra to reveal the mechanism of the novel optical properties of the nanocrystallites.

2. Experiment

The Pyrex glass (Na_2O–B_2O_3–SiO_2) with dispersed ZnS:Mn^{2+} nanocrystallites was prepared by a melting method. Na_2O–B_2O_3–SiO_2 and ZnS:Mn^{2+} (Mn^{2+}/ZnS = 1% (g/g)) powders were uniformly mixed and stirred. Then the mixture was heated at about 1300–1500 °C. After

§ Author to whom correspondence should be addressed.

0953-8984/99/275377+08$30.00 © 1999 IOP Publishing Ltd

Table 1. Some parameters and data of Pyrex glasses with dispersed ZnS:Mn^{2+} nanocrystallite.

	ZnS:Mn^{2+}/glass (wt%)	Emission peak (nm)	Max. in PLE spectrum (nm)	Diameter of nanocryst. (nm)	g_1 value	Param. of HFS, $\|A\|/g\beta$ (mT)	A_{up}/A_{down}
1	0.5	583, 423.4	303	3.4	2.0037 ± 0.0001	8.70 ± 0.01	0.73
2	10	575.8, 388.8	309.8	3.6	2.0035 ± 0.0001	8.41 ± 0.01	0.83
3	17	583.2	315.4	4.0	2.0034 ± 0.0001	8.33 ± 0.02	0.84
4	1	390	322				1.00
5	3	485					1.00
6	5	493					0.83
7	7	520			2.0050 ± 0.0005	8.49 ± 0.01	1.00
8	5 (ZnS/glass)	472					
9	ZnS:Mn^{2+} bulk powder	581	350.4		2.0027 ± 0.0001	6.99 ± 0.01	1.00

a time, the molten glasses containing ZnS:Mn^{2+} were cooled rapidly to room temperature to suppress the nucleation of ZnS:Mn^{2+} nanocrystallites. The glasses were annealed at 500 and 600 °C, respectively, to obtain samples with different sizes. The glasses obtained are transparent and uniform, colourless or light brown. As glasses containing even a small amount of Mn^{3+} are deep purple [5], our samples contain only Mn^{2+}. Some parameters of the samples are given in table 1.

The PL and PLE spectra of the samples were measured with a Hitachi F-4000 spectrometer at room temperature. EPR measurements were performed at room temperature with a spectrometer ESR 320 at 9.78 GHz.

3. Results and discussion

3.1. PL and PLE spectra

The PL spectra of samples 1, 2, 3 and 9 (bulk powder) are shown in figure 1. The F-4000 spectrometer has a 1.0 nm resolution and wavelength accuracy within ±2 nm. Although the PL spectra were not corrected, the resolution and accuracy are enough for broad band PL spectra measurement. The common feature of the samples is the observed orange emission from the $^4T_1$–$^6A_1$ transition (around 583 nm) of Mn^{2+}. The emission comes from the energy transfer from sp^3-hybridized orbital electrons of ZnS to d electrons of Mn^{2+}. It is suggested that Mn^{2+} substitutes Zn^{2+}. The $^4T_1$–$^6A_1$ emission bands are broadened for the following three reasons: (i) the size distribution of ZnS:Mn^{2+} nanoparticles, (ii) Mn^{2+} locate at different sites in ZnS:Mn^{2+} nanoparticles and (iii) the increase of electron–phonon coupling in ZnS:Mn^{2+} nanoparticles. The $^4T_2$, $^4A_1$–$^6A_1$ transitions maybe immersed in the $^4T_1$–$^6A_1$ broad emission bands for exciting in the gap of the host lattice. The $^4T_1$–$^6A_1$ emission peaks in samples 1 and 3 shift to the red. This experimental fact is consistent with: (i) the decrement undergone by the Mn^{2+}–s distance when the nanocrystal size decreases [6] and (ii) the diminution of the $^6A_1 \rightarrow {}^4T_1$ when the metal ligand distance increases [7]. Analysis of the reason that there is no red shift for sample 2 is further needed. 'Self-activated' (SA) luminescence at 423.4 nm caused by Zn vacancies (V_{Zn}) in the lattices was observed in sample 1 similar to 435 nm in [2]. With increasing Mn^{2+} concentration, SA luminescence disappears in emission spectra of samples 2–8 (see figures 1 and 3). The orange emissions from the $^4T_1$–$^6A_1$ transition of Mn^{2+} were not observed in samples 4, 5 and 6. This results from weak sp–d electron mixing or no energy transfer between matrix ZnS and Mn^{2+}. It is indicated that Mn^{2+} ions are not occupying Zn^{2+} sites, but may occupy interstitial sites, or $(Mn^{2+})_{int}$. As the calcining temperature increases over

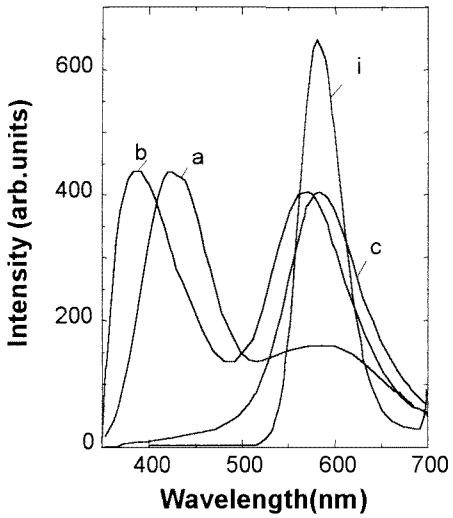

Figure 1. Emission spectra: a × 25 for sample 1, b × 25 for sample 2, c × 25 for sample 3 and i for sample 9.

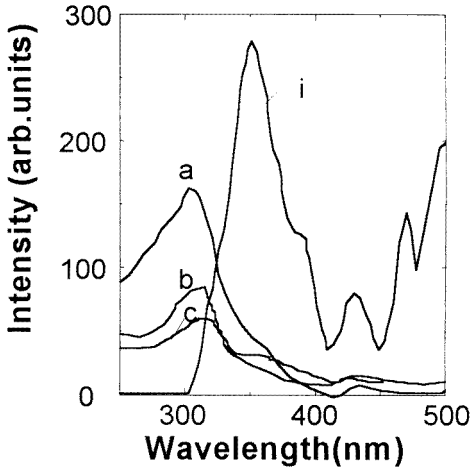

Figure 2. Excitation spectra: a × 10 for sample 1, b × 10 for sample 2, c × 10 for sample 3, i for sample 9.

950 °C, the phase of ZnS is a mixture of cubic and hexagonal [8]. In the cubic phase the lattice constant (σ) of ZnS is 5.41 Å. In the hexagonal $\sigma = 3.81$ Å in the a axis direction and $\sigma = 6.23$ Å in the c axis, respectively. As the ionic radius of Mn^{2+} is 0.91, even in the mixing phase Mn^{2+} may locate at the sites among molecules of ZnS, and between ZnS and glass. As a result, the $(Mn^{2+})_{int}$ configuration can be formed. Mn locates at the sites around ZnS:Mn^{2+}, or Mn-activated (outside) nanocrystals in solution [2, 9], which is only one of the cases of $(Mn^{2+})_{int}$.

The energy of the lowest excited electronic states, a blue shift with respect to the bulk band gap, as a function of nanoparticle diameter was given by Brus using the effective mass approximation [10]. The sizes of the nanoparticles of the samples (table 1) were calculated from the blue shifts in PLE spectra (figures 2 and 4), assuming $0.42m_e$ and $0.61m_e$ as the effective mass of the electron and the hole respectively and a dielectric constant of 8.0 in ZnS.

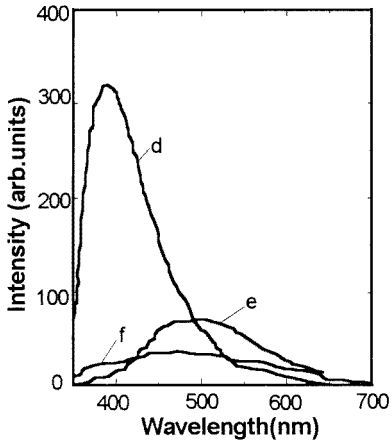

Figure 3. Emission spectra: d—sample 4, e—sample 5, f—sample 6.

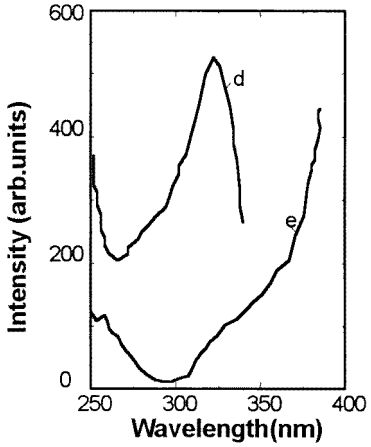

Figure 4. Excitation spectra: d—sample 4, e—sample 5.

3.2. EPR spectra

In order to verify the consequences obtained in the optical measurements, EPR experiments were carried out on the same samples at room and liquid nitrogen temperature, but there is no difference at both temperatures. The observation of signals of Mn^{2+} gives clear evidence of three kinds of site of Mn^{2+}. The EPR spectra of samples 1–9 (see figures 5 and 6) consist of three parts. The first part is a hyperfine sextet spectrum superposed on a broad background centred at about $g_1 = 2.0027$–2.0050. The six-line spectra result from Mn^{2+} occupying Zn^{2+} sites, or $(Mn^{2+})_{sub}$, called type II sites of Mn also in glass hosts [5]. Pure compounds of Mn^{2+} (such as $MnSO_4$ and $MnCl_2$ etc) above room temperature do not exhibit hyperfine structure as a result of exchange interaction between close Mn^{2+}. The unequal signal intensities of the hyperfine sextet demonstrate that the symmetry of Mn ions is lower than cubic phase and hexagonal phase is dominant. It is clear that at least a portion of these sites are characterized by crystal field effects small enough to be treated as perturbations. The second is the broad backgrounds that are attributed to the strong dipole–dipole interaction between Mn ions in

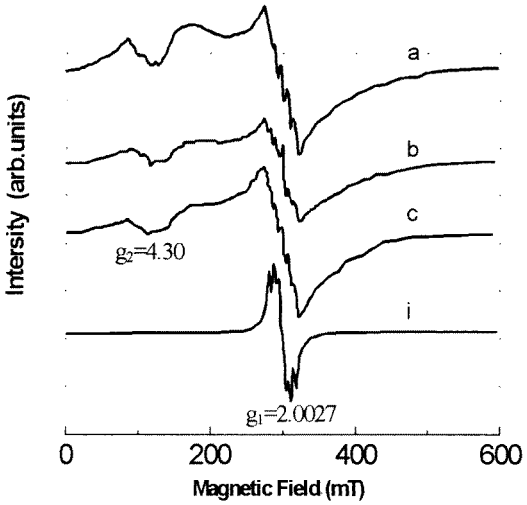

Figure 5. EPR spectra: a for sample 1, b for sample 2, c for sample 3 and i for sample 9.

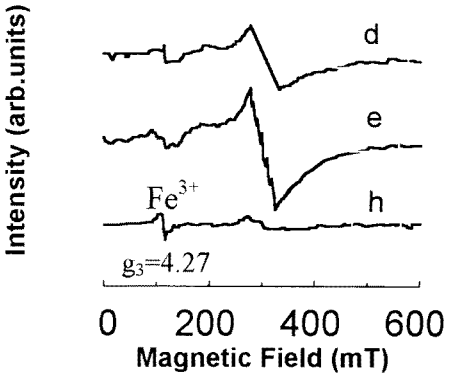

Figure 6. EPR spectra: d for sample 4, e for sample 5, h for sample 8.

clusters. To distinguish the contributions to EPR signal from the first and second parts, the six-line spectrum from $(Mn^{2+})_{sub}$ (figure 7 (C_1)) was subtracted from figure 5(c). The broad background assigned to the Mn cluster (figure 7 (C_2)) is predominant in figure 5(c). The third is that the wide bands centre at about $g_2 = 4.3$, resulting from $(Mn^{2+})_{int}$, denoted type-I sites of Mn in [5]. The EPR signals of Fe^{3+} with $3d^5$ electron configuration were also observed at about $g_3 = 4.27$ (figure 6(h)) similar to $g = 4.3$ of Mn^{2+} in Li_2O–B_2O_3 glasses containing more than 1 mol% Li_2O in [11]. The variations in amplitudes *A*, *B* and *C* (the inset in figure 8) in mm g^{-1} unit (mm: signal strength in EPR spectrum, g: sample's mass) with the percentages of ZnS:Mn^{2+} in Pyrex glasses are shown in figure 8. The contributions of Fe^{3+} were eliminated in the calculations for the amplitudes *C*. The amplitudes *A*, *B* and *C* can be thought of as proportional to the numbers of $(Mn^{2+})_{sub}$, Mn cluster and $(Mn^{2+})_{int}$, respectively. Below 10% composition of ZnS:Mn^{2+}, the amplitudes change slightly except sample 1. Two consequences about $(Mn^{2+})_{sub}$ can be drawn: (i) the amplitudes *A* for samples 1, 2 and 3 are greater than that of the others in figure 8, corresponding to the strong $^4T_1$–$^6A_1$ emissions of $(Mn^{2+})_{sub}$ (see figure 1(a)–(c)). (ii) If we draw a horizontal line through the centre of the EPR spectra for the

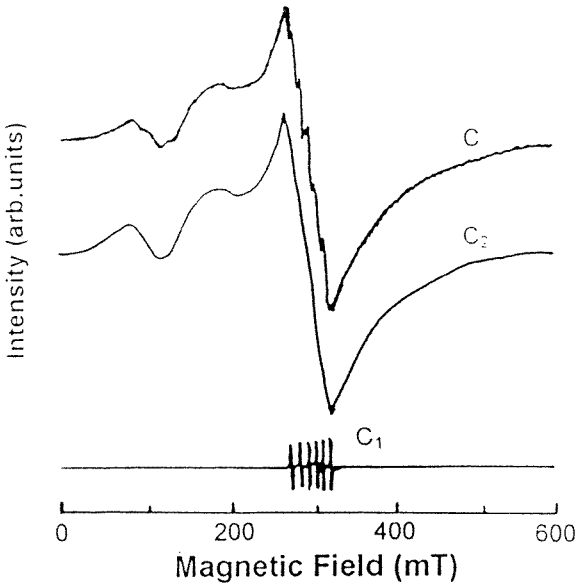

Figure 7. The EPR spectrum for sample 3 (figure 5(c)) is separated into two parts, $C = C_1 + C_2$.

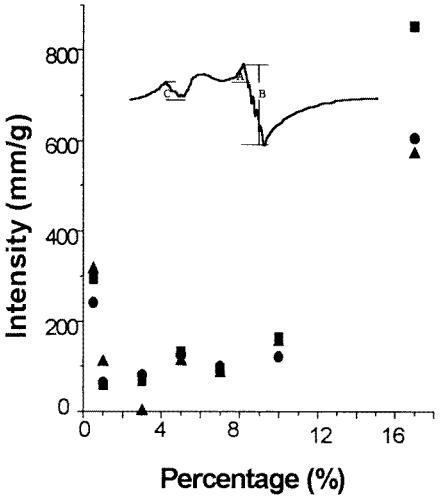

Figure 8. Intensity of EPR signals (mm g^{-1}) versus the percentages of ZnS:Mn^{2+} in Pyrex glasses, ●—*A*; ■—*B* (÷6); ▲—*C*.

samples, the square *A* (integral strength) of the EPR signal can be divided into two parts, A_{up} and A_{down}. The values of A_{up}/A_{down} are given in table 1. It is well known that the ^{4}G–^{6}S transition of Mn^{2+} is spin forbidden ($\Delta S = 1$). The perturbation by the crystal field makes the $^4T_1$–$^6A_1$ transition partially electric dipole allowed. The EPR signals for samples 1–3 have stronger symmetry breaks than the others with $A_{up}/A_{down} = 1$ (except the sample 6). This is consistent with the samples 1–3 with the strong $^4T_1$–$^6A_1$ emission in figure 1. The EPR spectrum for bulk powder (sample 9) has a good symmetry $A_{up}/A_{down} = 1$, but it has

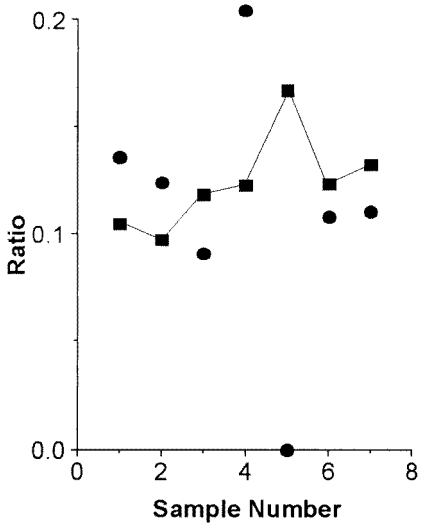

Figure 9. Ratio versus the sample numbers. ■—$A/(A + B + C)$; ●—$C/(A + B + C)$. The solid line is for guiding the eyes.

many more Mn^{2+} luminescence centres than the samples 1–3, so it still has the strong $^4T_1$–$^6A_1$ transition. We found that the amplitude B of the Mn cluster (divided by six in figure 8) is enhanced with increasing concentrations of Mn ions. The amplitudes B are greater than A and C in all samples (1–8) apparently. It is shown that most Mn ions were aggregated, forming Mn clusters during calcining. The sample 4 has a strong emission at 390 nm (figure 3(d)) from $(Mn^{2+})_{int}$. The ratio $C/(A + B + C)$ of sample 4, or the fraction of $(Mn^{2+})_{int}$ in the total Mn ions, is greater than the others, in figure 9.

The strengths of EPR signals are generally determined by the spin Hamiltonian, but, for nanoparticles, also by their sizes. The spin Hamiltonian appropriate for an Mn^{2+} ion ($S = 5/2$, $I = 5/2$) in the nanocrystals is given by [12, 13],

$$H = H_{Zee} + H_{HFS} + H_{cf} + H_{FS} = g\beta \boldsymbol{H} \cdot \boldsymbol{S} + \boldsymbol{A}\boldsymbol{S} \cdot \boldsymbol{I} + (1/6)a(S_x^4 + S_y^4 + S_z^4) + D[S_z^2 - (1/3)S(S+1)]. \quad (1)$$

The first term describes the Zeeman energy. H_{Zee} has the typical magnitude 0–1 cm^{-1}. The second term is concerned with the hyperfine structure produced by the interaction of nuclear spins with an unpaired electron. H_{HFS} is of value 0–10^{-2} cm^{-1}. The third term describes the cubic-field splitting observed in oriented single crystals. H_{cf} is concerned with high spin ($S \geqslant 3/2$). The fourth term is the fine structure splitting term resulting from spin–spin interaction. The fine structure term H_{FS} has the typical magnitude 0–1 cm^{-1}. EPR spectra of samples 1, 2, 3 and 9 are shown in figure 5. The EPR spectrum (figure 5(i)) of Mn^{2+} in ZnS powder with zincblende structure (tetrahedral symmetry of the centre) is mainly determined by the six HFS lines of the isotropic fine structure transition $|1/2, m\rangle$ to $|-1/2, m\rangle$. The g factor gives the information on situations of free and unbonded electrons. From the spectrum, $g_1 = 2.0027 \pm 0.0002$ and $|A| = 6.99 \pm 0.01$ mT were calculated. It is obvious that the symmetry of the microenvironment of Mn^{2+} in figure 5(a)–(c) is lower than that in figure 5(i). From sample 3 to 1 the diameters of the nanocrystals decrease, but g_1 factors (2.0034 ± 0.0002 to 2.0037 ± 0.0001) and HFS constants $|A|$(8.33 ± 0.02 to 8.70 ± 0.01 mT) increase. The latter increases more rapidly. As the hyperfine constant reflects the covalency of the bond between

Mn^{2+} and the ligand [14] this trend is consistent with the parallel increase experienced by the gap E_g which would lead to an increase of the ionicity. It is suggested that there are two reasons for the g shift Δg. One is the changes of the discrete energy levels of host ZnS due to the hybridization of s–p states of ZnS with d states of the Mn ions by quantum confinement effects. The other is that the surface/volume ratio increases as the size decreases; surface states (dangling bonds, defect sites etc) also play an important role in g shift.

4. Conclusions

To sum up, we have prepared Pyrex glasses with dispersed ZnS:Mn^{2+} nanocrystals. It is shown that Mn ions are situated at three different microenvironments, or $(Mn^{2+})_{sub}$, $(Mn^{2+})_{int}$ and Mn cluster respectively by the optical and EPR spectra. With decreasing diameters of the nanocrystals, g_1 factors and HFS constants increase. Quantum confinement and surface states result in the changes in g_1 factors and HFS constants.

Acknowledgments

The authors from the Changchun Institute of Physics, Chinese Academy of Sciences thank the National Foundation of Natural Sciences of China and Laboratory of Excited State Processes for funding.

References

[1] Bhargava R, Gallagher D, Hong X and Nurmikko A 1994 *Phys. Rev. Lett.* **72** 416
[2] Sooklal K, Cullum B, Angel S and Murphy C 1996 *J. Phys. Chem.* **100** 4551
[3] Yu J, Liu H, Wang Y, Fernandez F, Jia W, Sun L, Jin C, Li D, Liu J and Huang S 1997 *Opt. Lett.* **22** 913
[4] Liu J Y, Liu C X, Xu W and Li D 1997 *Sci. China* **42** 388
[5] Griscom D and Griscom R 1967 *J. Chem. Phys.* **47** 2711
[6] Soo Y L, Ming Z H, Hunag S W, Kao Y H, Bhaargava R N and Gallagher D 1994 *Phys. Rev.* B **50** 7602
[7] Rodriguez F and Moreno M 1986 *J. Chem. Phys.* **84** 692
[8] Lu W, Xu M and Huang W 1992 *Chin. J. Lumin.* **13** 355
[9] Gomez Sal J C, Rodriguez F, Moreno M and Tholence J L 1988 *Phys. Rev.* B **37** 454
[10] Brus L 1984 *J. Phys. Chem.* **80** 4403
[11] Castner T, Newell G S, Holton W C and Slichter C P 1960 *J. Chem. Phys.* **32** 668
[12] Kennedy T, Glaser E, Klein P and Bhargava R 1995 *Phys. Rev.* B **52** R14 356
[13] Poole C P Jr 1983 *Electron Spin Resonance* (New York: Wiley) p 8
[14] Simanek E and Muller K 1970 *J. Phys. Chem. Solids* **31** 1027